Silicification and dolomitization of anhydrite nodules in argillaceous terrestrial deposits: an example of meteoric-dominated diagenesis from the Triassic of central Spain

A. M. ALONSO-ZARZA , Y. SÁNCHEZ-MOYA , M. A. BUSTILLO A. SOPEÑA and A. DELGADO

ABSTRACT

Cauliflower-shaped nodules are widespread in a single red mudstone bed in the Buntsandstein (Triassic) facies of the Iberian Range. They consist mostly of quartz, dolomite and calcite, but other minerals, such as barite, kaolinite and iron oxyhydroxides, are also present. The nodules are spherical, ovoid or elongate in shape and range from 1 to 8 cm across. The surface of the nodules is irregular, and some show a pedogenic coating of microspar. The sedimentological and petrographic data suggest that the initial anhydrite nodules formed through a progressive increase in the porewater concentration of Ca^{2+} and SO_4^{2-} in a vadose environment, occasionally under the influence of pedogenic processes. Partial replacement of the anhydrite by megaquartz occurred under more dilute conditions in the same type of setting, as indicated by the presence of organic filaments on the quartz crystal surfaces. In type A nodules, the dissolution of the innermost anhydrite was complete, and different types of quartz cement filled the porosity. Fracturing and meteoric cementation by calcite and minor amounts of kaolinite were the latest processes affecting these nodules. In type B nodules, the dissolution of the anhydrite was incomplete, inhibiting quartz cementation and enabling later dolomitization of the anhydrite. Dolomitization appears to have been driven by sulphate reduction, as indicated by the presence of bacterial bodies within the dolomite crystals. Dedolomitization and precipitation of barite, kaolinite and calcite spar cements occurred later under the influence of meteoric solutions. The nodules may mark the former locations of the water table and provide evidence for an episode of highly evaporitic conditions throughout wide areas of the basin. Their occurrence reveals not only a complex diagenetic history but is also indicative of palaeogeographic and palaeoclimatic conditions.

Keywords Anhydrite nodules, meteoric diagenesis, silicification, Spain, sulphate-reduction dolomitization, Triassic.

INTRODUCTION

The replacement of anhydrite nodules by quartz and carbonates (very often dolomite) has been recognized in sedimentary rocks from the Precambrian to the Tertiary. These nodules have often been termed 'cauliflower nodules' because of their shape and colour. They are more common in marine than in terrestrial depositional environments. In the former, they appear in settings interpreted to be sabkhas (Chowns & Elkins, 1974), intertidal to shallow subtidal (Geeslin & Chafetz, 1982) and even in deeper subtidal overlain with evaporitic supratidal sediments (Elorza & Rodríguez-Lázaro, 1984; Maliva, 1987). In most cases, silicification and dolomitization are closely associated processes that occurred during early diagenesis. In terrestrial environments, these nodules have only been reported in playa-lake deposits (Tucker, 1976a).

Cauliflower nodules may serve as indicators of ancient shorelines (Chowns & Elkins, 1974), emersion surfaces (Gómez-Alday *et al.*, 1994), palaeoclimate (Tucker, 1976a; Elorza & Rodríguez-Lázaro, 1984) and as an evidence for hypersaline porewaters during early diagenesis (Maliva, 1987). The cauliflower nodules of the Triassic of the Iberian Range are of interest for several reasons. The Iberian Range nodules are restricted to a single, widespread bed of red mudstones within the Buntsandstein facies of the Iberian Range, so their formation was therefore under lithological and sedimentological control. The nodules occur in terrestrial deposits, associated with biogenic features, in which environment cauliflower nodules have rarely been described. The Iberian Range nodules also have a more complex mineralogy and structure than those commonly described in other cauliflower-like nodules.

The aim of this investigation was to decipher the sequence of sedimentary and diagenetic processes responsible for the formation of these nodules. Of particular interest was information that the cauliflower nodules might provide on palaeoclimate, tectonic regimes and the composition and levels of ancient groundwater.

STRATIGRAPHICAL AND SEDIMENTOLOGIC SETTING

The Triassic Basin of central Iberia was an extensional basin controlled by the movements of two main fault systems running NW–SE and SW–NE (Fig. 1). These fault systems formed during the last stages of the Hercynian movements. In the study area, the reconstruction of the Triassic Basin reveals two different domains: a north-eastern one, where the thickness of the Triassic deposits reaches 950 m; and a south-western one, in which maximum thickness is 200 m (Fig. 1, A–B section). These domains are separated by an important basal detachment, the movements of which were contemporary with sedimentation and were responsible for the variation in thickness along the basin. Back-faulting and widespread extensional processes, acting in the basin around the transition from the lower to the middle Triassic, led to an increase in the sedimentation area towards the west and south-west (Sopeña *et al.*, 1988).

The Triassic sedimentary record is composed of three lithologicaly distinctive stratigraphic successions (Fig. 1). The lower succession consists of red beds of fluvial origin (Buntsandstein) that rest unconformably on Hercynian or Permian basement. The intermediate succession consists of carbonates with intercalated detrital beds (Muschelkalk) that were deposited in shallow-marine environments. The upper succession (Keuper) is composed of evaporites, such as laminated and nodular gypsum and anhydrite, interbedded with detrital sediments. Intertidal carbonates of the Dolomías Tableadas de Imón Formation overlie the Keuper deposits. The total thickness of Mesozoic deposits overlying the Buntsandstein facies in the study area varies from 400 to 700 m.

The cauliflower nodules occur within Buntsandstein red beds. These facies consist of four fluvial units, designated C, Ss, S and Sm (Fig. 1), that were deposited in braided and meandering stream environments (Sopeña & Sánchez-Moya, 1997). The cauliflower nodules are located in the uppermost unit (Sm), which varies in thickness from 30 m in the W. Pálmaces section (Fig. 1, no. 2) to 10 m in the Cardeñosa section (Fig. 1, no. 8). The unit consists of massive mudstones and interbedded sandstones. The geometry of the sandstone beds varies from: (a) tabular beds with planar, slightly erosive bases and concave margins and internal fining-upwards sequences bounded by epsilon-like surfaces, corresponding to high-sinuosity channels within a meandering fluvial system; (b) thin, wide tabular beds showing parallel lamination and current ripples, corresponding to crevasse-splay deposits; and (c) bodies with planar bases and convex tops a few metres wide that correspond to levees of the channel margin. Unit Sm was deposited in a very

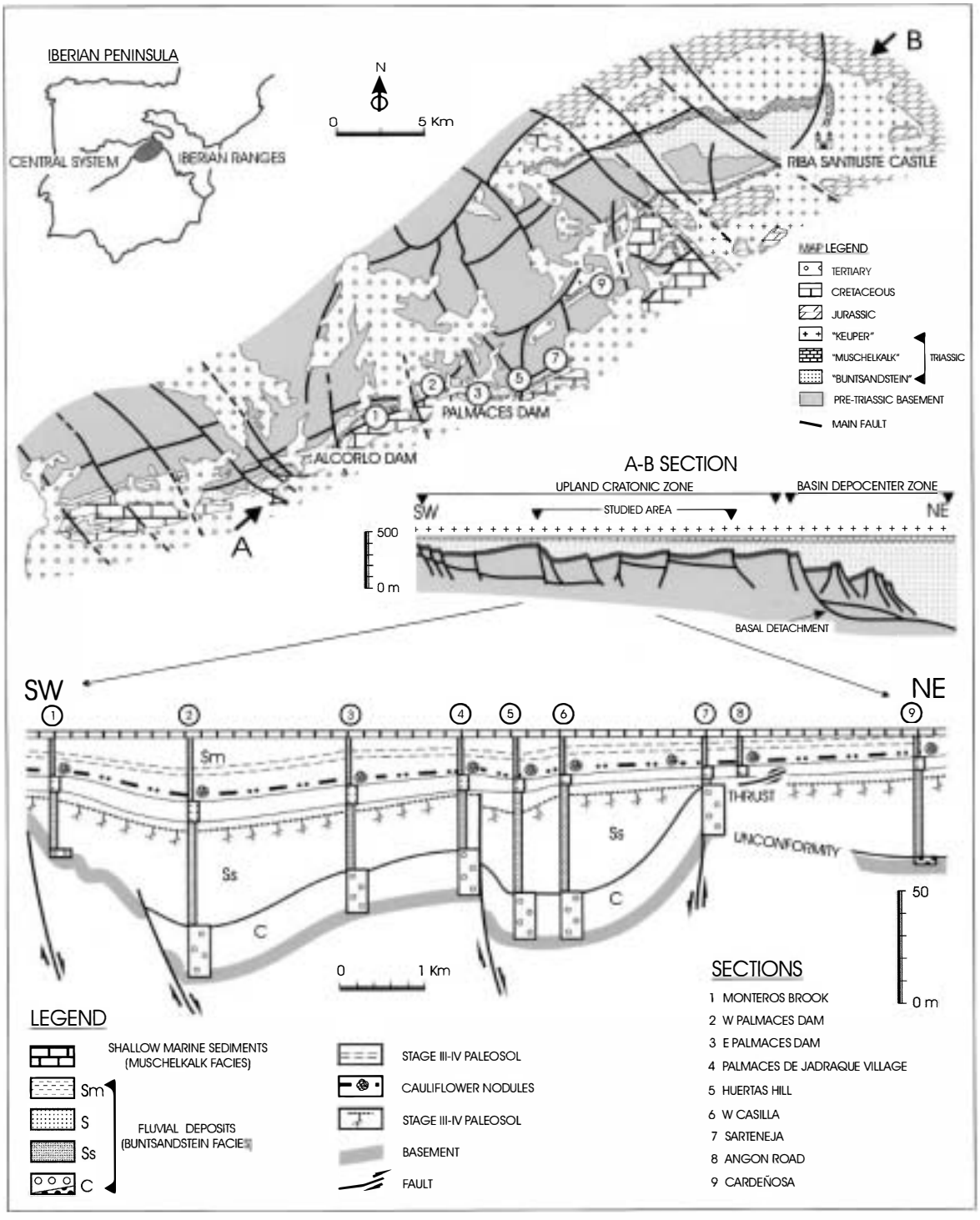

Fig. 1. Geological map, stratigraphy and main tectonic elements active during the Triassic sedimentation of the study area. The lower sketch shows simplified stratigraphic sections and the main stratigraphic units of the study area. The cauliflower-shaped nodules occur in a red mudstone bed in the Sm unit and are widespread throughout the area.

low-lying distal area with very narrow channels (ribbons) that occasionally meandered.

The transition to marine carbonates and terrigenous sediments (Muschelkalk) is relatively fast and is shown by 1–2 m of fining-upwards sequences at the topmost part of the unit. These sequences consist of mudstones and fine-grained sandstones with tidal lamination, occasional halite pseudomorphs and fine carbonate levels with 'tepee' structures. Similar facies and

sequence associations have been reported elsewhere in transitional environments (Diemer & Bridge, 1988; Muñoz *et al.*, 1992).

METHODS

The studied exposures of the cauliflower nodules were documented in previous investigations performed in the study area by Sopeña *et al.* (1995), Sánchez-Moya *et al.* (1997) and others. The nodules examined in the present study came from nine localities (Fig. 1). More than 100 nodules were cut in order to obtain polished hand specimens. Thin sections of 35 nodules were studied under transmitted light and cathodoluminescence (CL). Sample mineralogy was determined using a Philips XRD system operating at 40 kV and 30 mA with monochromated CuK_a radiation. Scanning electron microscopy (SEM) was performed with a JEOL 6·400 working at 20 kV; fracture surfaces were covered with gold, whereas polished surfaces were carbon-coated for back-scattered analyses. Microprobe analyses were performed with an EPMA using WDS, model JXA 8·900 (Jeol) from UCM. The standards used are described by Jarosewich *et al.* (1980) and were provided by the Smithsonian Institute, Washington, USA. Microprobe analyses concentrated on determining the proportions of the major element compositions within the different phases.

Isotope measurements were performed at the Stable Isotope Laboratory of the Estación Experimental del Zaidín (CSIC, Granada, Spain). Samples were ground to <200 mesh and treated with 100% phosphoric acid for 12 h in a thermostatic bath at 25 °C (McCrea, 1950). In samples containing calcite and dolomite, a double extraction at 25 °C and 50 °C was performed (Al-Aasm *et al.*, 1990). Acid fractionation factors used were 1·01044 at 25 °C for calcite (Kim & O'Neil, 1997) and 1·01065 at 50 °C for dolomite (Rosenbaum & Sheppard, 1986). Isotopic ratios were measured by a Finnigan MAT 251 mass spectrometer. The experimental error for carbonates ($\delta^{13}C$ and $\delta^{18}O$) was ± 0·1‰, using Carrara and EEZ-1 as internal standards previously calibrated to NBS-18 and NBS-19.

OCCURRENCE OF THE CAULIFLOWER-LIKE NODULES

As mentioned above, the cauliflower nodules occur scattered in the lowermost part of unit Sm (Fig. 1). The bed containing the nodules extends for more than 30 km. Within the red mudstone bed, the nodules show a general horizontal trend. The mudstone bed consists of illite within a microcrystalline mosaic of dolomite crystals and includes variable amounts of etched detrital grains, such as quartz and feldspars. The mudstone bed was deposited in the floodplain of a meandering river system.

PETROLOGY

The nodules are spherical, ovoid or, in some cases, elongate. They range from 1 to 8 cm across. Their surfaces are irregular and have a 'cauliflower' shape (Fig. 2). Some nodules are composed of several smaller nodules separated by films of red to green clays cemented by dolomite. The outer surface of the nodules is red or, less commonly, green. Some nodules show a discontinuous cortex of several millimetres of laminated micropseudospar calcite.

Many of the nodules show a concentric structure defined by a succession of different types of quartz and carbonate phases (Fig. 3A and B). Other nodules lack the concentric structure because a network of fractures resulted in the brecciation of the nodule. The nodules are composed of quartz (30–100%), calcite (5–70%), dolomite (0–35%), anhydrite (0–5%), barite (0–5%), kaolinite (0–5%) and goethite (0–5%).

Fig. 2. External morphology of a cauliflower-shaped nodule.

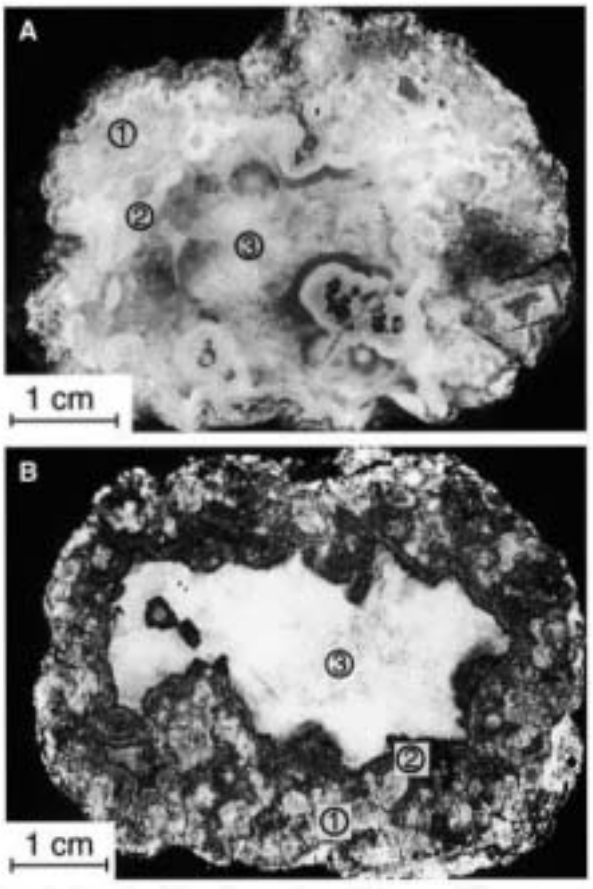

Fig. 3. Polished hand samples of the cauliflower nodules. (A) Type A nodule showing: 1, megaquartz; 2, quartzine and fibrous quartz; 3, calcite cement. (B) Type B nodule showing: 1, megaquartz; 2, zoned dolomite; 3, calcite cement.

Petrography

The outer carbonate cortex

Some quartz nodules show a discontinuous cortex of microspar several millimetres thick. The microspar laminae consist of calcite crystals (40 μm across). The laminae have spheroidal to ovoid pores (Fig. 4A) of <1 mm across and ghosts of micritic filaments. This cortex also includes etched detrital quartz and feldspar grains as well as clays.

Quartz fabrics and textures

Quartz forms the outermost part of the nodules (Fig. 4B–E) and, in a few cases, the whole nodule. Quartz shows two textures: megaquartz and length-slow chalcedony (quartzine), both of which may occur as fragments within nodules (Fig. 4F). In nodules containing both textures, megaquartz occupies the outermost part, whereas quartzine is located towards the interior (Figs 4B and 5A). Megaquartz, which is the most abundant quartz phase, occurs as single euhedral crystals and inequigranular mosaics of clusters of crystals in a carbonate matrix as well as in bands of elongated crystals.

The inequigranular mosaics consist of subhedral to euhedral crystals (Fig. 4B) that vary in size from 0·03 to 3 mm across. The crystals display unit or undulose extinction (flamboyant and microflamboyant quartz). These features are typical of the megaquartz formed by replacement of sulphates (Milliken, 1979; Arbey, 1980). Anhydrite inclusions are only seen in the megaquartz with homogeneous extinction, and they are commonly disordered within crystals. Inclusions tend to be more prevalent along the external parts of the nodules.

The single and clusters of euhedral crystals (Fig. 4A) are mainly hexagonal bipyramidal and up to 4 mm long (Fig. 5B). The quartz crystals commonly contain anhydrite inclusions that are either: (a) organized as bands parallel to the crystal faces (Fig. 5B); (b) concentrated in the central part of the crystals (Fig. 5C); or (c) disorganized and scattered throughout the crystals. The quartz crystals are isolated within mosaics of calcite or dolomite in the most central part of the nodules (Fig. 5D).

Under SEM, the external surface of the quartz crystals exhibits very regular and flat surfaces to irregular surfaces enclosing relics of anhydrite (Fig. 5E) and incipient corrosion by carbonates. The regular surfaces can include large organic filaments hundred of microns long and about 2 μm across (Fig. 5E and F). In some samples, the relatively regular and flat surfaces have circular structures about 70 μm in diameter (Fig. 5G and H) that are probably produced by dissolution of a fibrous rim of quartzine that enveloped the external area or the euhedral quartz crystals. Spherical to ovoid bodies of dolomite, about 1 μm in diameter, probably bacterial in origin, are present on the megaquartz surfaces (Fig. 6A).

Elongated (acicular, palisadic or columnar) megaquartz crystals form thin bands in the inner part of the nodule (Fig. 6B). The crystals are about 0·2 mm long, 30 μm in width and are perpendicular to the surfaces on which they lie. The crystals and their arrangement clearly resemble drusy cements.

Quartzine is less common than megaquartz and is only seen in nodules with a relatively thick ring of quartz. Quartzine commonly occurs as

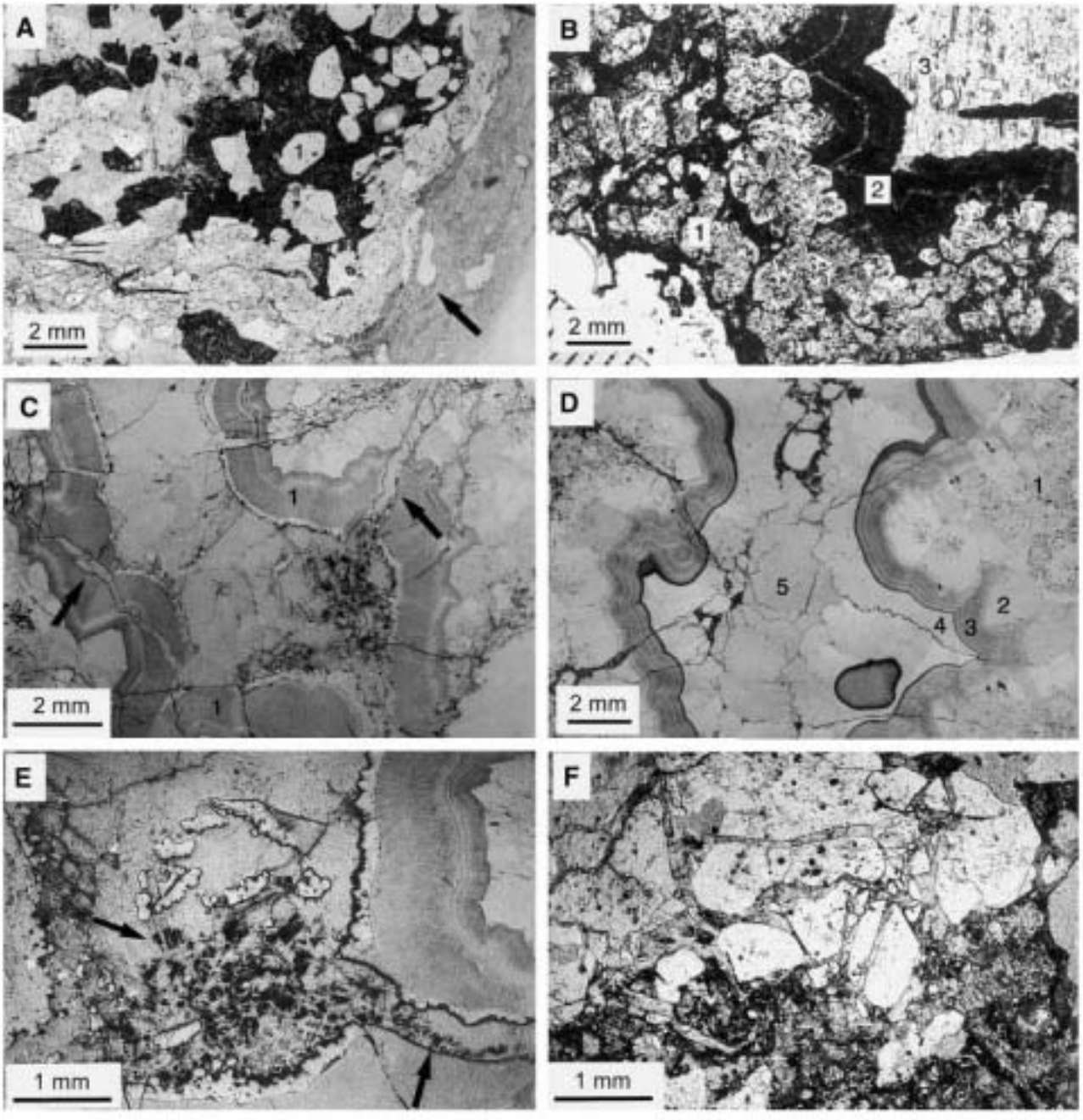

Fig. 4. Photomicrographs. (A) View of part of a nodule showing an outer part of laminated micrite with alveolar structure (arrowed) and euhedral megaquartz crystals (1) within a dark dolomite. (B) View of a complete sequence of a type B nodule consisting of euhedral megaquartz crystals within dolomite (1), zoned dedolomite (2) and late calcite spar cement (3). (C) Type A nodule lacking the dolomite part and showing a rim of quartzine (1). The nodules contain fractures (arrowed) and late calcite spar cement (in the centre of the nodule). (D) A complete sequence of a type A nodule showing, from the outermost part to the centre: megaquartz crystals with anhydrite inclusions (1), megaquartz with few or lacking anhydrite inclusions (2), a rim of quartzine (3), a rim of palisadic quartz (4; see Fig. 6B for detail) and calcite spar cement (5). (E) View of (C) showing fractures filled by calcite spar cement and kaolinite (arrowed). (F) View of a highly fractured nodule, looking like a quartz breccia cemented by dolomite.

rims up to 2 mm thick coating megaquartz mosaics (Fig. 6B) and single crystals. Under transmitted light, the rims and spherulites are beige to brown on account of the presence of small iron inclusions, as indicated by microprobe analyses (13% FeO). Locally, the quartzine rims or the elongated quartz crystals are coated with fan-like arrangements of goethite. In broken nodules, all

the described textures appear as fragments cemented by calcite (Fig. 4F), overall forming a breccia.

Carbonate fabrics and textures

Dolomite occurs as bands in the inner part of the nodules (Figs 3B and 4B) and as mosaics of euhedral dolomite crystals up to 4 mm in length, which may include euhedral quartz (Fig. 5D). The quartz–dolomite contact is sharp, and signs of corrosion of quartz by dolomite, such as dissolution embayments within the quartz, are uncommon. Under CL, dolomite is orange and commonly luminesces brightly. Dolomite is ferroan ($Ca_{49\cdot1}Mg_{47\cdot3}Fe_{3\cdot5}C\bullet_3$) and, locally, a richer iron phase similar to ankerite ($Ca_{63}Mg_3Fe_{34}C\bullet_3$) was detected by the microprobe. In most cases, the dolomite has undergone dedolomitization, which appears to have concentrated iron/manganese on some crystal faces and produced some crystals showing alternate calcite and dolomite zones (Fig. 6C). Dolomite and calcite after dolomite are absent in nodules that contain rims of quartzine.

Inclusions of anhydrite occur in the dolomite mosaics. In some cases, the inclusions were leached, and only their moulds are preserved, either empty or filled by calcite. Under SEM, the dolomite crystals show textures indicating partial dissolution and, in some cases, dedolomitization. Some organic structures, such as spherical bodies of about 1 μm in diameter (bacteria), as well as large filaments, occur within the dolomite crystals (Fig. 6D).

Calcite occurs as a replacement of dolomite or as cement. The mean composition of calcite cements is $Ca_{99\cdot1}Mg_{0\cdot71}Fe_{0\cdot2}C\bullet_3$, whereas calcite that replaced dolomite is enriched in Mg and Fe ($Ca_{95-99}Mg_{3\cdot5-1\cdot5}Fe_{1-0\cdot15}C\bullet_3$). Calcite formed through replacement of dolomite occurs as euhedral mosaics that include the quartz crystals. The calcite crystals have some bands enriched in goethite and have a high intracrystalline porosity. Evidence of a dolomitic precursor includes: the rhombic morphology of the crystals and the preservation of dolomite within some zones of the crystals. Calcite cements are composed of euhedral to subeuhedral limpid calcite crystals, which vary in size from 10 μm to 5 mm, increasing towards the centre of the nodule. These calcite cements occur: (a) in the innermost part of the nodules, filling the central void (Figs 3A, B and 4E); (b) in fracture porosity (Fig. 4F); and (c) filling the moldic porosity left by the dissolution of anhydrite inclusions within quartz and dolomite crystals. CL images have shown that these mosaics have bright orange luminescence and dark zones.

Sulphates

Anhydrite (about 100 μm across) is only present as inclusions within the megaquartz and dolomite. In the dolomite mosaics, inclusions are sparse and show no preferred distribution. The distribution pattern of the inclusions within the quartz mosaics and euhedral crystals was described above.

Barite occurs as lenticular to tabular crystals up to 5 mm long (Fig. 6E). These crystals may be isolated or connected to each other forming incipient 'desert roses' within calcite. Barite occurs only in nodules that originally contained dolomite. Barite shows signs of corrosion and is encased by optically continuous calcite, and hence predates calcite.

Kaolinite

Kaolinite was identified based on chemical composition (40·3% $Si\bullet_2$ and 36·57% $Al_2\bullet_3$) and X-ray diffraction (XRD) patterns. The crystals are about 30 μm long, and form fans of ≈0·4 mm in diameter (Fig. 6E). They are present near the contact between the last silica phase and the carbonate phases, and either in fractures through the siliceous part of the nodules or in the innermost part of the nodules (Fig. 4E).

Goethite

Much of the goethite occurs as thin bands parallel to the faces of the carbonate crystals. Goethite occurs as 3-μm-diameter crystals with a flower- or spherulite-like texture. In nodules containing a large inner zone of dolomite, square morphologies suggestive of oxidized pyrites are present locally. Goethite also occurs along the external boundary of the quartzine rims or at the contact between silica or carbonate phases and the late calcite cement. Bustillo *et al.* (1999) described large haematite crystals in quartz nodules of similar age. These were not seen in the present study area.

Host rock relics

Relics of red mudstone are present within the nodules, mostly at the contact between the siliceous and carbonate phases. These preserved relics of the host rock contain some biogenic

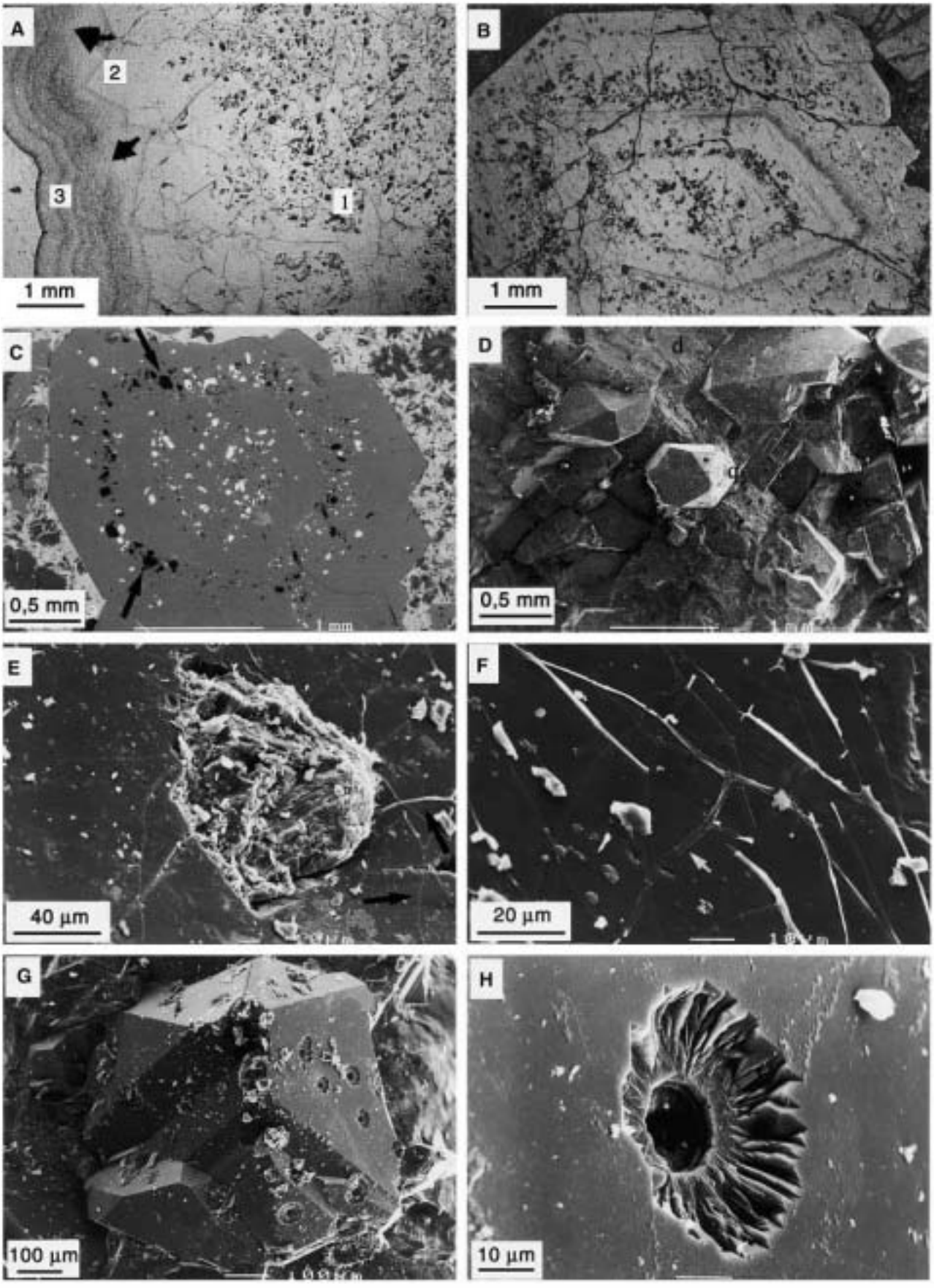
A
2
3
1
1 mm
B
1 mm
C
0,5 mm
D
d
0,5 mm
E
40 µm
F
20 µm
G
100 µm
H
10 µm

Fig. 5. (A) Arrangement of different quartz phases within a nodule, from the exterior to the interior: megaquartz with a large amount of anhydrite inclusions (1), megaquartz lacking anhydrite inclusions (2), and rim of banded quartzine (3). (B) Euhedral quartz showing different phases of growth indicated by the organized inclusions of anhydrite. (C) Back-scattered image of a megaquartz crystal revealing a homogeneous composition, even when the anhydrite bands suggest different growth phases. Anhydrite inclusions are concentrated in the centre of the crystal and in a band towards the exterior of the megaquartz, where many of them have been leached (arrowed). (D) SEM image of the inner part of a nodule. The euhedral megaquartz (q) is embedded within a coarse dolomite mosaic (d). (E) SEM image of the surface of a megaquartz crystal with an inclusion of partially dissolved anhydrite and some organic fungal (?) filaments (arrowed). (F) SEM image of the surface of a megaquartz crystal coated by a number of organic filaments. (G) SEM image of a euhedral megaquartz crystal showing some peculiar dissolution features. (H) Detailed view of one of the solution features of (G).

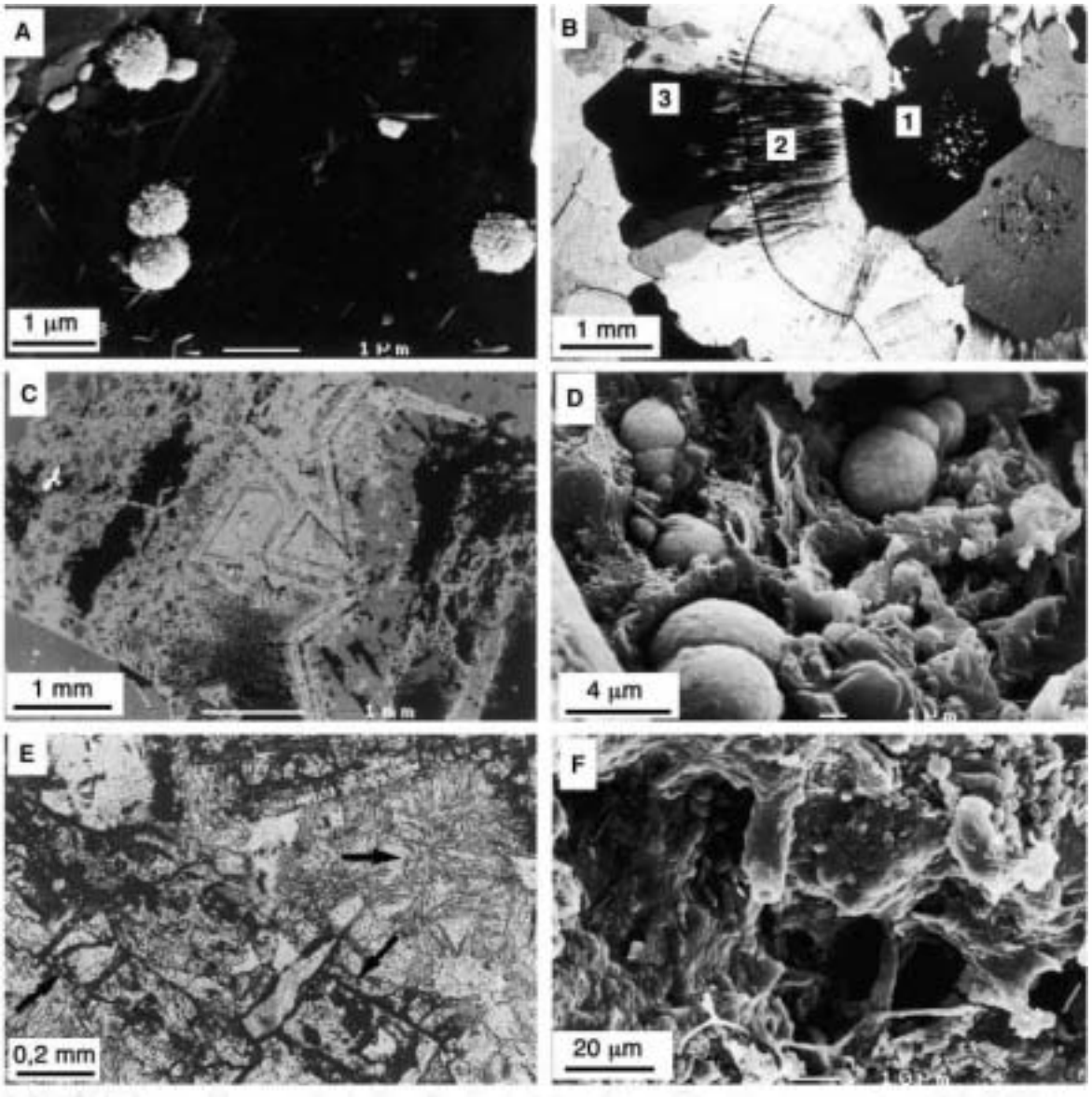

Fig. 6. (A) SEM image of some spherical bodies (bacteria) on the surface of a megaquartz crystal. (B) Photomicrograph of a sequence of: megaquartz (1), quartzine (2) and palisadic quartz (3) (detailed view of Fig. 4B under crossnichols). (C) Back-scattered image of compositional zoning within dedolomitized areas; darker bands correspond to Ca-rich carbonate (calcite after dedolomitization) and darker areas to relics of dolomite. (D) SEM image of the dolomite crystals including some spherical bodies and some long and straight filaments. (E) Photomicrograph of barite crystals (arrows) and kaolinite towards the upper right angle (also arrowed). Kaolinite crystals are arranged in fan-like aggregates and embedded in calcite spar cement. (F) SEM image of the host rock; some organic tubes and filaments are still preserved within the dolomitic red mudstones.

structures, probably fungal filaments, which have not collapsed (Fig. 6F). Some etched detrital grains such as quartz and feldspars are also present.

ISOTOPE GEOCHEMISTRY

Stable isotope analyses were carried out on the calcite and dolomite of the nodules. Seventeen samples were analysed, all of them containing calcite, and five containing dolomite as well (Fig. 7). In calcites, either cement or replacing dolomite, $\delta^{13}C$ values vary between –9·2‰ and –6·3‰, and $\delta^{18}O$ between –7·4‰ and –4·8‰. In dolomites, $\delta^{13}C$ values range from –7·7‰ to –5·1‰ and from –7·8‰ to –6·1‰ for $\delta^{18}O$. In samples containing both calcite and dolomite, the $\delta^{18}O$ values in dolomite are lighter (average 0·8‰) than those obtained in the same sample from calcite.

INTERPRETATION OF THE DIAGENETIC SEQUENCE

The different textures recognized, their arrangement and the geochemical data allow the interpretation of the sequence of diagenetic processes that formed these nodules (Fig. 8).

Formation of anhydrite nodules

The morphology of the nodules and the presence of anhydrite inclusions in the quartz and dolomite indicate that the nodules had an anhydrite precursor. In terrestrial settings, anhydrite nodules are found in playa-lake environments (Rodríguez-Aranda *et al.*, 1991; Salvany *et al.*, 1994), in pedogenic profiles such as gypcretes from the Miocene of Chile (Hartley & May, 1998) or in palustrine evaporite settings such as in the Miocene Calatayud Basin in Spain (Sanz-Rubio *et al.*, 1999). In these environments, anhydrite can precipitate directly within capillary saline solutions (Kinsman, 1974; Rodríguez-Aranda, 1995) in the presence of some organic compounds, which promotes anhydrite precipitation (Cody & Hull, 1980). In the study case, the pedogenic cortex and the presence of organic structures (fungi) in the outer part of the nodules indicate that the nodules formed in a surficial vadose environment. The widespread distribution of the nodules in the basin, as demonstrated by the presence of similar nodules in the same bed over a distance of >35 km (Bustillo *et al.*, 1999), strongly indicates the presence of a single continuous water table.

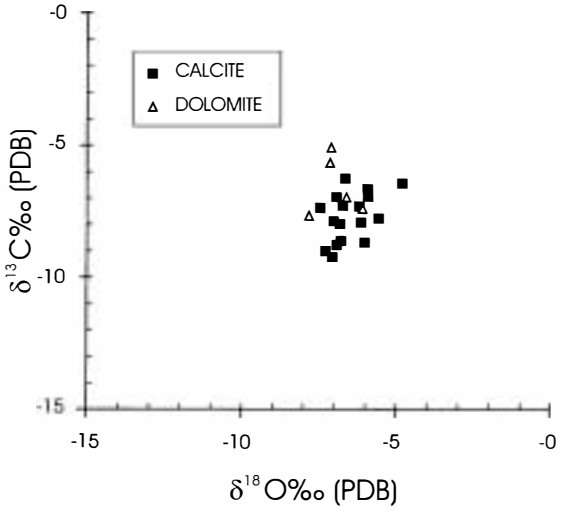

Fig. 7. Cross-plot of $\delta^{18}O$–$\delta^{13}C$ values of the calcite and dolomite of the cauliflower nodules.

Formation of carbonate coatings

The morphology and arrangement of the pores and laminations seen in these coatings are similar to structures formed by calcification of root structures and associated microorganisms (Mack & James, 1992; Alonso-Zarza, 1999). The recrystallized fabric of the coatings and the lack of any relationship with the current water table indicate that they are not recent. These coatings probably formed by pedogenic processes at very nearly the same time as the anhydrite nodules.

Silicification

The presence of anhydrite inclusions concentrated in the outer parts of the nodules is the main argument for the nodules having formed by the replacement of an anhydrite precursor, which proceeded from the outside inwards. The presence of quartz mosaics with a considerable amount of scattered anhydrite inclusions may indicate a volume-for-volume replacement of anhydrite by silica in the initial stages. In a subsequent stage, the rate of anhydrite dissolution exceeded quartz precipitation, producing secondary porosity (Chowns & Elkins, 1974). The increasing sulphate dissolution allowed growth of the quartz crystals in a less dense mass of sulphate and so favoured the organiza-

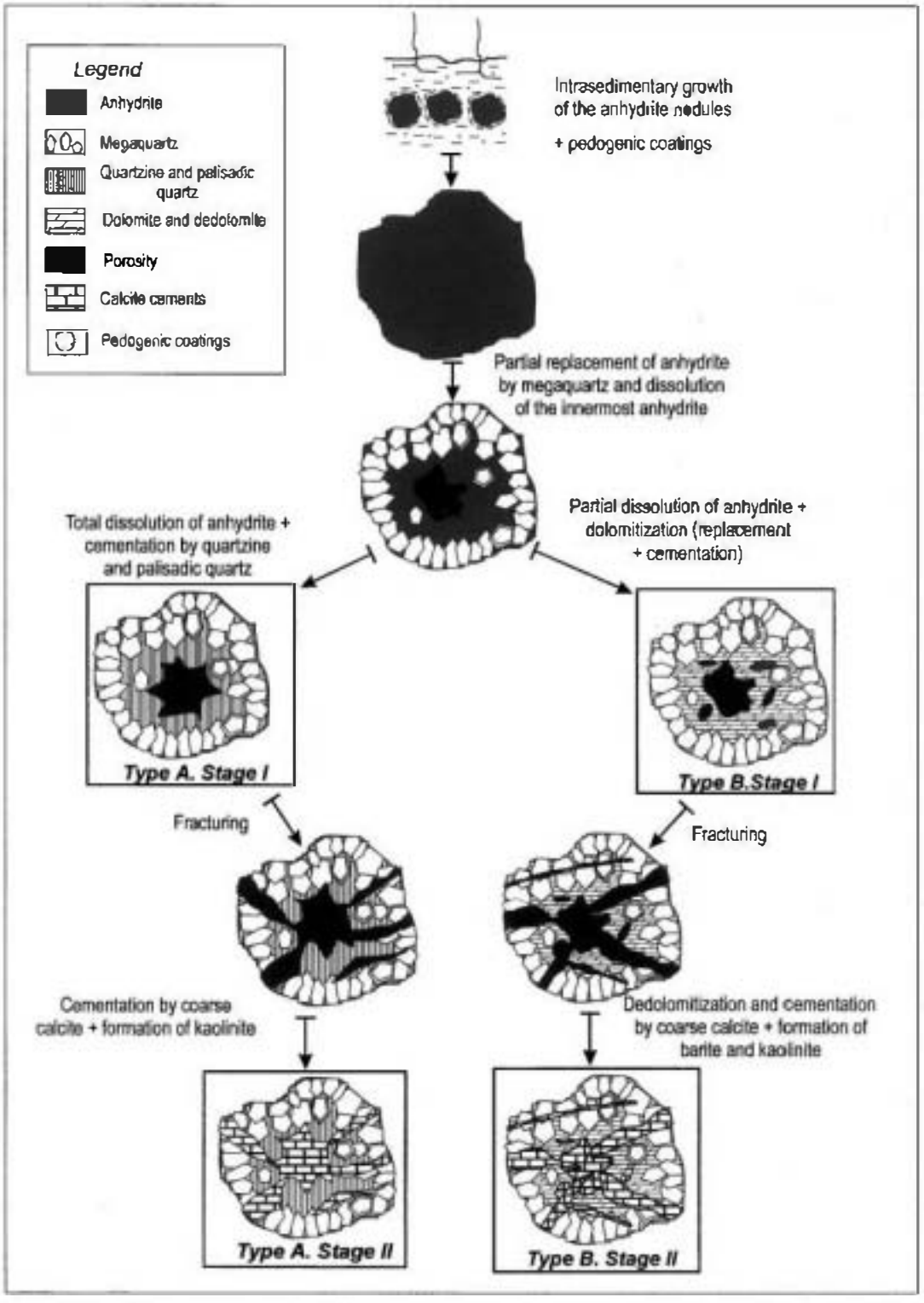

Fig. 6. Sketch of the diagenetic evolution of the anhydrite nodules. Boxed nodules indicate stages of evolution that have been identified in the nodules.

tion of inclusions conforming to the euhedral shape of the growing quartz crystals (Tucker, 1976a).

After the initial replacement and dissolution of the anhydrite, two general diagenetic sequences can be recognized (Fig. 8). In type A nodules, the

complete dissolution of anhydrite enabled the precipitation of quartz and calcite cements. Drusy quartz lacking anhydrite inclusions occurs in the innermost part of the nodules and represents the first clear quartz cement (Fig. 8, type A, stage I). Bands of quartzine constitute the last phase of quartz cementation. In type B nodules, the process of silicification ends with the formation of megaquartz crystals with the remaining anhydrite replaced by dolomite (Fig. 8, type B, stage I).

The dissolution and replacement of anhydrite by quartz is indicative of the circulation of groundwaters supersaturated in silica and the low availability of sulphates (Tucker, 1976a). Folk & Pittman (1971) and Siedlecka (1976) considered that high pH or sulphate-rich environments favoured the presence of megaquartz and quartzine. The silica concentration of the groundwater was controlled by the pH. Under alkaline conditions, detrital quartz and other silicates of the red mudstones or adjacent red clastic deposits can be dissolved, increasing the silica concentration in the groundwater, and a slight decrease in pH enabled their precipitation. Fibrous quartz textures, present in the innermost part of some nodules, are indicative of precipitation from solutions with higher silica concentrations than the mosaics of megaquartz crystals (Milliken, 1979). Therefore, the sequence of quartz textures suggests precipitation from solutions with increasing silica concentration.

The replacement of anhydrite by quartz has been considered an early diagenetic process in shallow-marine and terrestrial environments (e.g. Tucker, 1976a,b; Geeslin & Chafetz, 1982; Maliva, 1987, among others). Only exceptionally, and based on the presence of hydrocarbon inclusions in megaquartz, has silicification of anhydrite nodules been interpreted as a burial diagenetic process (Ulmer-Scholle *et al.*, 1993). In the present case, the presence of organic filaments on the surfaces of some euhedral crystals (Fig. 5F), similar to the fungal filaments described by Feldmann *et al.* (1997), suggests that silicification was an early diagenetic process that occurred with no significant burial.

Dolomitization

Dolomitization is very commonly associated with silicified anhydrite nodules. It can be earlier (Maliva, 1987), concomitant (García-Garmilla & Elorza, 1996) or later than silicification (Friedman & Shukla, 1980). In the present case, dolomite engulfs and corrodes the quartz crystals and fills cavities either within the quartz crystals or in the inner part of the nodules. All these features indicate that dolomitization occurred after silicification.

Three observations have to be considered when interpreting the dolomitization process: (i) there was no previous carbonate phase, and dolomitization occurred replacing anhydrite; (ii) bacterial bodies and organic filaments are present within the dolomite crystals; (iii) only the nodules in which the anhydrite was not totally leached contain dolomite. These observations suggest that dolomitization was driven by bacterial sulphate reduction of the remaining anhydrite or of sulphate ions present in the groundwaters. In this process, two moles of $2HCO_3^-$ are released for each mole of SO_4^{2-} reduced (Berner, 1980; Wright, 1999). Sulphate reduction may promote dolomitization by: (a) removal of the dissolved SO_4^{2-}, which may act as an inhibitor of dolomitization; (b) production of alkalinity; and (c) production of NH_4^+, which may release adsorbed Mg^{2+} (Baker & Kastner, 1981). Dolomitization by sulphate-reducing bacteria is currently a matter of discussion and may be more important than previously thought (Burns *et al.*, 2000).

Although the $\delta^{13}C$ values obtained for the dolomites formed through this process may vary from negative to strongly positive (Mazzullo, 2000), the isotopic composition of the nodules (Fig. 7) fits well with the wide range of values of organogenic dolomites formed by sulphate reduction. In our case, the negative $\delta^{13}C$ values indicate an important contribution of ^{12}C from degraded organic matter. Morad *et al.* (1992) have suggested that the influence of carbon derived from soil organic matter may, among other causes, explain the low $\delta^{13}C$ values of the dolomitic cements of the Buntsandstein sandstones. In addition, dolomite and calcite (either cement or dedolomite) show different isotopic values, indicating that their formation took place in waters of different composition. The lighter values of dolomite may suggest a more organic control of their formation than in the formation of calcite.

Fracturing

Some nodules contain fractures that affect all the quartz textures and the dolomite. However, the outer part of the nodule did not collapse (Fig. 8). Angular quartz fragments (breccias) formed as the result of the fracturing and are now cemented by

calcite. Calcite cements precipitated in fractures could contribute to the enlargement of the fractures.

Calcite spar cementation, dedolomitization, barite and kaolinite precipitation

The close association of calcite cements, dedolomitization, kaolinite and barite suggests the input of relatively fresh, dilute and oxygenated waters of meteoric origin. Calcite, either cement or dedolomite, has light oxygen isotopic values (Fig. 7), which point to a meteoric origin. Dedolomitization accounts not only for the replacement of dolomite, but also for the dissolution of relic anhydrite in the dolomite. Dedolomitization of these iron-rich dolomites resulted in iron-poor calcite and the precipitation of iron oxyhydroxides parallel to the calcite crystal faces. Iron can accumulate in the boundaries between any quartz phase and late calcite cements or on the boundary between dolomite/dedolomite and the last calcite cement.

Barite is fairly common in quartz nodules and may also occur in association with celestite (Siedlecka, 1972). Celestite is absent in the nodules. Barite occurs only in nodules that contain dolomite or calcite after dolomite (Fig. 8), which suggests that sulphate came from the dissolution of the anhydrite inclusions of the dolomite. Barite solubility calculations demonstrate that changes in salinity cause variations in the barium sulphate activity coefficient (Monnin, 1999). Thus, a decrease in the salinity causes an increase in the activity coefficient and favours the precipitation of the barite. In the studied nodules, barite precipitation was favoured by the input of freshwaters. These freshwaters may also have carried different ions from the drainage of the uplands (Palaeozoic massif and Triassic sediments), which contained a variety of epithermal minerals including barite (Concha *et al.*, 1992).

Kaolinite has hardly ever been reported in this type of nodule. Only Scholle *et al.* (1992) have described kaolinite 'booklets' within blocky calcite spar in calcite-replaced evaporite rosettes from the Delaware Basin. However, the association of barite and kaolinite is not rare in clastic deposits that have undergone early diagenesis under the influence of acidic, meteoric porewaters and the decay of organic matter (Diekmann & Wopfner, 1996). Aluminium required for kaolinite precipitation could also come from the weathering of feldspars in the red mudstones, and the relics of organic structures still present in the nodules might have favoured their mobility.

PALAEOENVIRONMENTAL CONTROLS ON THE OCCURRENCE OF CAULIFLOWER-LIKE NODULES

The presence of the quartz cauliflower-like nodules has been used to infer data about the position of the coastline and also as evidence for a change from a transgressive to a regressive situation (Chown & Elkins, 1974). Moreover, these nodules have been used to indicate relatively arid climates (Folk & Pittman, 1971; Siedlecka, 1976; Tucker, 1976b). The detailed sedimentology carried out on the nodule bed, its position within the basin and its own characteristics provide some information about the climatic and tectonic conditions that prevailed during their formation.

Climate

The nodules are restricted to just one bed within the Sm unit. This unit represents the deposition of ephemeral and meandering fluvial systems under a semi-arid climate with marked seasonality (Muñoz *et al.*, 1992; Sánchez-Moya *et al.*, 1997). At this time, precipitation was sporadic and was followed by dry periods and subsequent evaporation. During evaporative periods, capillary rise of phreatic waters occurred through the highly permeable orange conglomerates and sandstones of unit S (Fig. 1). Thus, oversaturation of calcium sulphate occurred within the vadose zone. The nodule bed may indicate either more intense evaporative processes or longer, drier periods.

Tectonism

The cauliflower-like nodules are found over a wide area of the Triassic basin. The bed can be followed for more than 35 km. Moreover, this bed, which was only examined in the cratonic area in the present study (Fig. 1), continues into the more subsiding areas of the basin. This suggests that the area was relatively flat, and tectonic activity was at a minimum. This would account for the stabilization of the groundwater table, leading to the basinwide distribution of these nodules at the same stratigraphic level. Thus, the presence of the cauliflower-like nodules reflects episodes of tectonic stability and low relief, related in time to the expansion of the

Triassic basin. At this stage, the sedimentation area was wider and compartmentalization of the basin minimal. The occurrence of these beds in the sedimentary record may be used as a correlation tool in continental fluvial settings.

CONCLUSIONS

The Buntsandstein deposits of central Spain contain a red mudstone bed, in which quartz cauliflower nodules after anhydrite can be found throughout the fluvial basin. These nodules show complex patterns of replacement and cementation textures by mostly quartz and carbonates. The original anhydrite nodules probably formed during a period of evaporative concentration by capillary rise. The nodules formed within the vadose zone, occasionally under the influence of pedogenic processes. Soon after their formation, and under more dilute conditions possibly related to wetter periods, the anhydrite was partially replaced by megaquartz. This replacement took place under surficial conditions, as indicated by the presence of a number of fungal filaments on the quartz surface. From this point, their diagenetic evolution is more complex and dependent on the presence or absence of anhydrite. Nodules in which anhydrite dissolution was complete (type A) followed a simpler diagenetic path. Replacement by megaquartz was followed by quartz cementation (quartzine and palisadic quartz), fracturing and a late phase of calcite spar cementation occasionally containing kaolinite. Nodules in which anhydrite was not totally leached (type B) lack quartz cements and underwent dolomitization that was driven by sulphate reduction. Dedolomitization, calcite spar cementation and barite precipitation are the latest processes to affect these nodules.

As this bed is present across most of the Triassic basin, it may be used in correlation. These nodules offer information not only on their diagenetic history, but also on the climatic and tectonic conditions that resulted in their extensive formation across the fluvial basin.

ACKNOWLEDGEMENTS

This work was supported by project PB97-1208 of DGES and also by PB98-0668-C02-0. The authors wish to thank G. Herrero for his special care in making the thin sections. Members of the Petrology Department also contributed with suggestions on the identification of silicate minerals and textures. Robert Maliva, Dana Ulmer-Scholle and an anonymous reviewer improved the paper through their suggested revisions. Peter Mozley is thanked for his editorial work.

REFERENCES

Al-Aasm, I.S., Taylor, B.E. and **South, B.** (1990) Stable isotope analysis of multiple carbonate samples using selective acid extraction. *Chem. Geol.*, **80**, 119–125.

Alonso-Zarza, A.M. (1999) Initial stages of laminar calcrete formation by roots: examples from the Neogene of central Spain. *Sed. Geol.*, **126**, 177–191.

Arbey, F. (1980) Les formes de la silice et l'identification des évaporites dans les formations silicifiées. *Bull. Centres Rech. Explor.-Prod. Elf-Aquitaine*, **4**, 309–365.

Baker, P.A. and **Kastner, M.** (1981) Constraints on the formation of sedimentary dolomite. *Nature*, **213**, 214–216.

Berner, R.A. (1980) *Early Diagenesis – A Theoretical Approach*. Princeton University Press, New Jersey, 241 pp.

Burns, S.J., McKenzie, J.A. and **Vasconcelos, C.** (2000) Dolomite formation and biogeochemical cycles in the Phanerozoic. *Sedimentology*, **47 (Suppl. 1)**, 49–61.

Bustillo, M.A., García-Guinea, J., Martínez-Frías, J. and **Delgado, A.** (1999) Unusual sedimentary geodes filled by gold-bearing hematite laths. *Geol. Mag.*, **136**, 671–679.

Chowns, T.M. and **Elkins, J.E.** (1974) The origin of quartz geodes and cauliflower cherts through the silicification of anhydrite nodules. *J. Sed. Petrol.*, **44**, 885–903.

Cody, R.D. and **Hull, A.B.** (1980) Experimental growth of primary anhydrite at low temperatures and water salinities. *Geology*, **8**, 505–509.

Concha, A., Oyarzun, R., Lunar, R., Sierra, J., Doblas, M. and **Lillo, J.** (1992) The Hiendelaencina epithermal silver-base metal district, Central Spain: tectonic and mineralizing processes. *Mineral. Deposita*, **27**, 83–89.

Diekmann, B. and **Wopfner, H.** (1996) Petrographic and diagenetic signatures of climatic change in peri- and post-glacial Karoo Sediments of SW Tanzania. *Palaeogeogr. Palaeoclimatol. Palaeoecol.*, **125**, 5–25.

Diemer, J.A. and **Bridge, J.S.** (1988) Transition from alluvial plain to tide-dominated coastal deposits associated with the Tournaisian marine transgression in SW Ireland. In: *Tide-Influenced Sedimentary Environments and Facies. Sedimentology and Petroleum Geology* (Eds P.L. de Boer, A. van Gelder and S.D. Nio), pp. 359–388. Reidel Publishing, Dordrecht.

Elorza, J. and **Rodríguez-Lázaro, J.** (1984) Late Cretaceous quartz geodes after anhydrite from Burgos, Spain. *Geol. Mag.*, **121**, 107–113.

Feldmann, M., Neher, J., Jung, W. and **Graf, F.** (1997) Fungal quartz weathering and iron crystallite formation in an Alpine environment, Piz Alv, Switzerland. *Eclogae Geol. Helv.*, **90**, 541–556.

Folk, R.L. and **Pittman, J.S.** (1971) Length-slow chalcedony: a new testament for vanished evaporites. *J. Sed. Petrol.*, **41**, 1045–1058.

Friedman, G.M. and **Shukla, V.** (1980) Significance of authigenic quartz euhedra after sulphates: example from the

Lockport Formation (Middle Silurian) of New York. *J. Sed. Petrol.*, **50**, 1299–1304.

García-Garmilla, G. and **Elorza, J.** (1996) Dolomitization and synsedimentary SALT tectonics: the Upper Cretaceous Cueva Formation at El Ribero, northern Spain. *Geol. Mag.*, **133**, 721–737.

Geeslin, J.H. and **Chafetz, H.S.** (1982) Ordovician Aleman Ribbon Cherts: an example of silicification prior to carbonate lithification. *J. Sed. Petrol.*, **52**, 1283–1293.

Gómez-Alday, J.J., García-Garmilla, F. and **Elorza, J.** (1994) Caracterización de las geodas de cuarzo de Laño (Sur de Vitoria). Relación con la actividad somerizante del diapiro de Peñacerrada (cuenca Vasco-Cantábrica). *Geogaceta*, **16**, 132–135.

Hartley, A.J. and **May, G.** (1998) Miocene Gypcretes from the Calama Basin, northern Chile. *Sedimentology*, **45**, 351–364.

Jarosewich, E.J., Nelen, J.A. and **Norberg, J.A.** (1980) Reference samples for electron microprobe analysis. *Geostandards Newsl.*, **4**, 43–47.

Kim, S.T. and **O'Neil, J.R.** (1997) Equilibrium and nonequilibrium oxygen isotope effects in synthetic carbonates. *Geochim. Cosmochim. Acta*, **61**, 3461–3475.

Kinsman, D.J.J. (1974) Calcium sulphate minerals of evaporite deposits: their primary mineralogy. *4th Symposium on Salt*, Northern Ohio, pp. 343–348.

McCrea, J.M. (1950) On the isotopic chemistry of carbonates and a paleotemperature scale. *J. Chem. Phys.*, **18**, 849–857.

Mack, G.H. and **James, W.C.** (1992) Calcic paleosols of the Plio-Pleistocene Camp Rice and Palomas Formation, southern Rio Grande rift, USA *Sed.* Geol., **77**, 89–109.

Maliva, R.G. (1987) Quartz geodes: early diagenetic silicified anhydrite nodules related to dolomitization. *J. Sed. Petrol.*, **57**, 1054–1059.

Mazzullo, S.J. (2000) Organogenic dolomitization in peritidal to deep-sea sediments. *J. Sed. Res.*, **70**, 10–23.

Milliken, K.L. (1979) The silicified evaporite syndrome –two aspects of silicification history of former evaporite nodules from southern Kentucky and northern Tennessee. *J. Sed. Petrol.*, **49**, 245–256.

Monnin, Ch (1999) A thermodynamic model for the solubility of barite and celestite in electrolyte solutions and seawater to 200°C and to 1 kbar. *Chem. Geol.*, **153**, 187–209.

Morad, S., Marfil, R., Al-Aasm, I.S. and **Gómez-Gras, D.** (1992) The role of mixing-zone dolomitization in sandstone cementation: evidence from the Triassic Buntsandstein, the Iberian Range, Spain. *Sed. Geol.*, **80**, 53–65.

Muñoz, A., Ramos, A., Sánchez-Moya, Y. and **Sopeña, A.** (1992) Evolving fluvial architecture during a marine transgression: Upper Buntsandstein, Triassic, central Spain. *Sed. Geol.*, **75**, 257–281.

Rodríguez-Aranda, J.P. (1995) *Sedimentología de los Sistemas de Llanura Lutítica-Lago Salino del Mioceno en la Zona Oriental de la Cuenca de Madrid (Tarancón-Auñon).* Doctoral Thesis, Universidad Complutense de Madrid.

Rodríguez-Aranda, J.P., Calvo, J.P. and **Ordoñez, S.** (1991) Transición de abanicos aluviales a evaporitas en el Mioceno del borde oriental de la Cuenca de Madrid (Sector de Barajas de Melo-Illana). *Rev. Soc. Geol. Esp.*, **4**, 33–50.

Rosenbaum, J. and **Sheppard, S.M.F.** (1986) An isotopic study of siderites, dolomites and ankerites at high temperatures. *Geochim. Cosmochim. Acta*, **50**, 1147–1150.

Salvany, J.M., Muñoz, A. and **Pérez, A.** (1994) Nonmarine evaporitic sedimentation and associated diagenetic processes of the southwestern margin of the Ebro Basin (Lower Miocene), Spain. *J. Sed. Res.*, **64**, 190–203.

Sánchez-Moya, Y., Sopeña, A. and **Ramos, A.** (1997) Infill architecture of a nonmarine half-graben Triassic Basin (Central Spain). *J. Sed. Res.*, **66**, 1122–1136.

Sanz-Rubio, E., Hoyos, M., Calvo, J.P. and **Rouchy, J.M.** (1999) Nodular anhydrite growth controlled by pedogenic structures in evaporite lake formations. *Sed. Geol.*, **125**, 195–203.

Schelle, P.A., Ulmer, D.S. and **Melim, L.A.** (1992) Late-stage calcites in the Permian Capitan Formation and its equivalent, Delaware Basin margin, west Texas and New Mexico: evidence for replacement of precursor evaporites. *Sedimentology*, **39**, 207–234.

Siedlecka, A. (1972) Length-slow chalcedony and relicts of sulphates – evidence of evaporitic environments in the upper Carboniferous and Permian red beds of Bear Island, Svalbard. *J. Sed. Petrol.*, **42**, 812–816.

Siedlecka, A. (1976) Silicified Precambrian evaporite nodules from northern Norway: a preliminary report. *Sed. Geol.*, **16**, 161–175.

Sopeña, A. and **Sánchez-Moya, Y.** (1997) Tectonic systems tract and depositional architecture of western border of the Triassic Iberian Trough (Central Spain). *Sed. Geol.*, **113**, 245–267.

Sopeña, A., Lopez, J., Arche, A., Perez, M., Ramos, A., Virgili, C. and **Hernando, S.** (1988) Permian and Triassic Rift basins of the Iberian Peninsula. *Dev. Geotectonics*, **22B**, 757–786.

Sopeña, A., Doubinger, J., Ramos, A. and **Pérez-Arlucea, M.** (1995) Palynologie du Permien et du Trias dans le Centre de la Péninsule Ibérique. *Sci. Géol. Bull.*, **48**, 119–157.

Tucker, M.E. (1976a) Quartz replaced anhydrite nodules ('Bristol Diamonds') from the Triassic of the Bristol District. *Geol. Mag.*, **113**, 569–574.

Tucker, M.E. (1976b) Replaced evaporites from the late Precambrian of Finnmark, Arctic Norway. *Sed. Geol.*, **16**, 193–204.

Ulmer-Scholle, D., Scholle, P.A. and **Brady, P.V.** (1993) Silicification of evaporites in Permian (Guadalupian) back-reef carbonates of the Delaware Basin, West Texas and New Mexico. *J. Sed. Petrol.*, **63**, 955–965.

Wright, D.T. (1999) The role of sulphate-reducing bacteria and cyanobacteria in dolomite formation in distal ephemeral lakes of the Coorong region, South Australia. *Sed. Geol.*, **126**, 147–157.